



Fatigue crack initiation in cold spray coated AZ31B-H24 with AA7075 powder

Bahareh Marzbanrad, Ehsan Toyserkani, Hamid Jahed *

Mechanical and Mechatronics Engineering Department, University of Waterloo, Canada



ARTICLE INFO

Keywords:

Cold spray
Residual stress
Fatigue
Cracking mechanism
Magnesium alloys
Aluminum powder

ABSTRACT

The effect of cold spray coating parameters on the fatigue life and cracking mechanism of AZ31B-H24 coated with AA7075 powder is investigated. Two sets of coated samples are fabricated based on the selection of different coating parameters. An in-situ control of heat transfer is performed to obtain different residual stress states and microstructure at the aluminum/magnesium interface. Subsequently, the samples are tested under load-controlled fatigue tests at different load amplitudes. Fatigue lives are obtained and the cracking behavior of the two samples is studied and compared with that of uncoated baseline samples. It is revealed that the samples with compressive residual stress at the coating/substrate interface have significantly longer lives (approximately 85% improvement at the same stress) compared with that of the baseline samples. In contrast, samples with tensile residual stress at the interface have similar or slightly improved lives (approximately 24%) compared with that of the baseline samples. The cracking mechanisms of these two samples are considerably different. In the case of compressive samples, cracks initiate at the coating surface and propagate through the splat boundaries of the cold spray coating to the substrate. Conversely, in the case of tensile samples, delamination and cracking initiate at the interface and subsequently propagate to the substrate and through the splats in the coating. The different lives and cracking mechanisms obtained are attributed to the differences in the initial state of stress, details of the microstructure of the nano-size interface layer, and the morphology of the substrate grains adjacent to the interface.

1. Introduction

Phenomena, such as climate change, global warming, and depleting energy resources, have led to significant research efforts to reduce the carbon footprint. A substantial portion of greenhouse gas emissions is directly emitted due to the transportation sector. Therefore, decreasing the weight of the mobile structures to reduce the fuel consumption has become a significant priority in automotive and aerospace industries. Recently, magnesium (Mg) and its alloys have attracted significant attention as the lightest structural materials with the highest strength-to-weight ratio among all commercially available metals [1]. However, the application of Mg alloys is restricted to non-load-bearing components due to shortcomings, such as low fatigue strength, poor corrosion characteristics, and wear resistance [2]. Coating the surface of manufactured parts with a thin layer of material with higher corrosion-and-fatigue-resistance is considered as a practical surface-modification approach to enhance the surface properties and durability of Mg alloys [3].

In an ideal condition, coating a defect-free layer of a tough and hard material with an acceptable cyclic work hardenability and good adherence can enhance the fatigue life of the substrate, regardless of the deposition technique. The fatigue life is improved owing to delay in fatigue crack initiation and propagation [4–6]. However, the coating surface is prone to defects. The presence of coating defects, such as voids, cracks, undeformed particles, surface imperfections, and tensile residual stress, in the coating or at the interface can have a detrimental effect on the durability of the coated samples [7–13]. It has been demonstrated that the fatigue crack initiation at the interface, which leads to the delamination of the coating and failure of the sample, is a critical problem that severely affects the fatigue life of coated samples [14]. Defects at the interface, poor splat toughness, and poor bonding between the substrate and coating along with the presence of tensile residual stress at the interface region can result in premature cracking in this particular area [4,7,13]. Moreover, it has been reported that the coated samples are susceptible to interfacial cracking at high-stress levels [12–14]. To address this issue, compressive residual stress is

* Corresponding author.

E-mail address: hjahedmo@uwaterloo.ca (H. Jahed).

induced in the coating surface using post-processing techniques, such as shot peening and/or grit blasting. This induction can transfer the crack initiation from the interface to the coating surface, which can considerably delay the crack initiation [5,6,15–17]. Therefore, altering the residual stress at the interface during the coating process can be an effective method to transfer the fatigue crack initiation from the interface to the surface of the coated layer and enhance the fatigue life of the coated samples.

Solid-state cold spray coating can form a dense coating layer without introducing the deleterious effects of alternative high-temperature coating methods, such as oxidation, evaporation, melting, phase transformation, and detrimental residual stresses [18–19]. In cold spraying, a coating layer is formed due to the high kinetic energy of micron-sized coating particles. The particles are supersonically accelerated by passing through a relatively low temperature and pressurized gas via a de Laval nozzle to impact and adhere to a substrate rather than using thermal energy for binding. Intensive plastic deformation of particles upon impact results in the mechanical and metallurgical bonding of the particles with the substrate [20]. The impingement of particles with high kinetic energy during the process can induce compressive residual stress in coated samples. However, an increase in thermal energy of the system due to the carrier gas, particle deformation upon impact, and thermal mismatch effects can provide destructive conditions and reverse the residual stress from negative to positive stress [21–22]. This situation can be highlighted for temperature-sensitive materials, such as Mg alloys [23].

Although cold spraying technology can enhance the fatigue resistance of materials, the fatigue behavior of Mg alloy coated samples has not been extensively investigated [24–27]. Cavaliere et al. [25] investigated the effect of processing parameters on the residual stress and fatigue performance of Al2024/AZ91 coated samples. The effect of carrier gas pressure and temperature, and particle speed in the coating microstructure, porosity, bonding strength, and residual stress formation were investigated. It was demonstrated that an increase in the carrier gas temperature and pressure increased the surface compressive residual stress, and improved the mechanical properties and fatigue limit of the coated samples [25]. In contrast, the temperature of the system was considered as a dominant effect that induced tensile residual stress in cold spray additively manufactured hollow titanium cylinders [28]. It was concluded that the thermal stresses were overcome due to the peening effects at a lower nozzle speed. Therefore, a significant tensile residual stress was developed near the outer and inner surfaces of the cylinder [28]. Dayani et al. [27] studied the fatigue behavior of AZ31B cast Mg alloy samples coated with AA7075 powder. The residual stress profiles of the coated samples revealed that significant compressive residual stress was induced in the coating, and a tensile residual stress of 12 MPa was induced at the substrate interface. The higher hardness and fatigue strength of the coating material on the substrate and the induced compressive residual stress of the coating enhanced 25% the fatigue strength of the coated samples at 10^7 cycles compared with that of as-received samples. The examination of fracture surfaces exhibited delamination and cracking at the interface. It was observed that primary cracks were initiated and propagated from the substrate due to pores and casting defects on the Mg side of the interface [27]. The pores and casting defects might cause primary crack initiation. However, the presence of tensile residual stress in the substrate due to thermal mismatch and substrate microstructural changes due to high thermal energy can cause an undesirable crack initiation from the substrate [29–30].

The residual stress of AZ31B-H24 substrate near the interface after the deposition AA7075 was customized [31]. The coating parameters, particularly coating temperature, was altered to induce a significant compressive residual stress in the coating and substrate interface [23,31]. It was observed that the Mg-coated samples with compressive residual stress exhibited enhanced mechanical properties, such as higher hardness of the coating and interface, lower porosity and surface

roughness, and finer grain microstructure, compared with that of samples with tensile residual stress [23,29].

This research aims to study the effect of cold spray coating parameters on the fatigue crack mechanism and fatigue resistance of AA7075/AZ31B-H24 coated samples. Two different samples were fabricated using different coating setups and parameters. Coated samples with tensile and compressive residual stress at the substrate/coating interface were fabricated. Fatigue tests were performed to determine the fatigue life of the tensile and compressive specimens. The crack initiation locations in the tensile and compressive samples before failure were identified and compared. The cause of crack initiation was discussed in detail.

2. Experimental procedure

2.1. Materials

Fifty rectangular samples of AZ31B-H24 Mg alloy sheet with dimensions of 70×12.5 mm and thickness of 3.16 mm were used as the substrates. The dimensions of the samples were determined based on the guidelines provided in the ASTM D790 test method. The samples were stress-relieved at $260^\circ\text{C}/15$ min following the procedure recommended by ASM to ensure that the substrates were stress-free [32]. Thus, it was ensured that the residual stresses observed after coating were solely due to the cold spray process.

A spherical-shaped commercial AA7075 powder (supplied by Centerline Ltd., Windsor, Canada) was used for the coating. The average radius of the powder particles was measured as $23 \mu\text{m}$ using the Retsch Technology, Camsizer XT. Fig. 1a and b depict the SEM image of the powder and the particle size distribution, respectively. The chemical compositions of AZ31B-H24 Mg alloy [33] and AA7075 coating material, which were measured by a Bruker energy-dispersive X-ray spectroscopy (EDS), are listed in Table 1.

2.2. Design of experiment

Residual stresses are the byproduct of cold spray coating and additive manufacturing [34–35]. The distribution of these residual stresses can significantly affect the characteristics of the coating and substrate near the interface [29]. Two sets of specimens were designed to examine the effect of residual stresses on the cracking mechanism of coated samples under cyclic load. The resultant residual stress at the substrate interface due to the coating was considered as the input variable for the investigation of the fatigue life of coated samples. Additionally, the cracking mechanism was considered as the response (output variable). Marzbanrad et al. [22–23] demonstrated the effect of cold spray deposition parameters on the formation and distribution of residual stresses in the coating and in the substrate near the interface. Two sets of cold spray deposition parameters were selected using these results to design two different specimens. The first type of sample consisted of compressive residual stress in the coating and substrate (herein called compressive sample). The second type of sample consisted of compressive residual stress at the coating surface that transitioned to tensile residual stress in the coating and were transferred through the interface to the substrate (herein called tensile sample). The heat transfer between the coating and substrate can be used to control the residual stress induced during cold spray coating [29].

2.3. Coating process

A commercial supersonic spray technologies (SST) series P cold spray system (Centerline, Windsor, Canada) was used for depositing AA7075 on the Mg alloy samples. The coating parameters were selected to control the induced residual stress based on the two types of specimens designed for this study. The selection of the parameters was based on earlier studies [23,29]. Table 2 lists the coating processing parameters

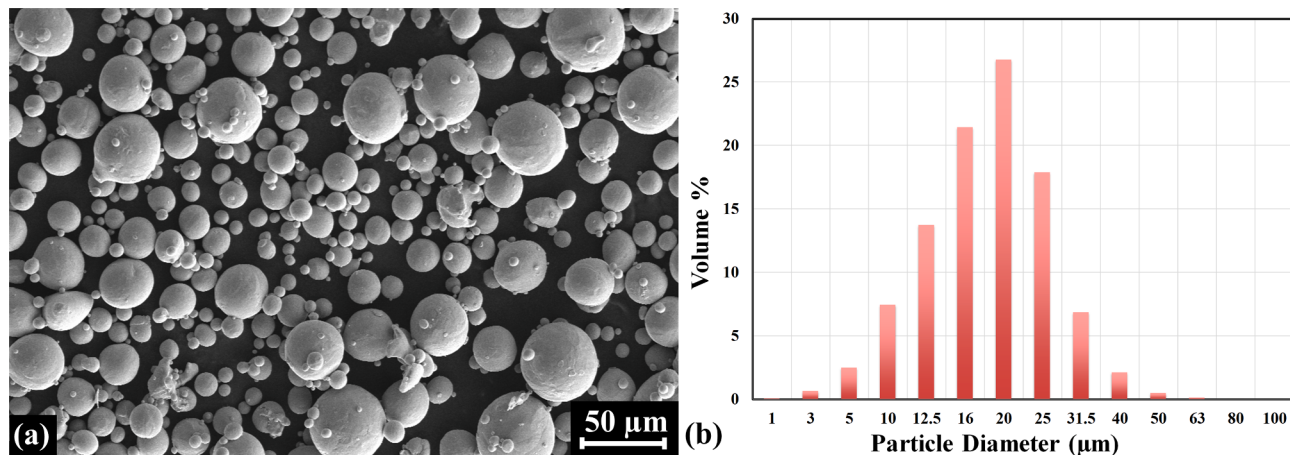


Fig. 1. a) SEM image. b) Particle size distribution for AA7075 powder.

Table 1
Chemical composition of AZ31B-H24 [33] and AA7075.

Composition (Weight%)	Aluminum (Al)	Zinc (Zn)	Manganese (Mn)	Iron (Fe)	Nickel (Ni)	Silicon (Si)	Copper (Cu)	Chromium (Cr)	Magnesium (Mg)	Other elements
AA7075	90	5.20	–	0.35	0.005	–	1.55	0.25	2.35	0.30
AZ31B-H24	2.99	0.95	0.2 min	0.005	–	0.05	0.05	–	Bal.	–

Table 2
Cold spray processing parameters.

Coating process	Carrier gas	Gas temperature (°C)	Gas pressure (MPa)	Feed rate (gr/min)	Nozzle speed (mm/s)	Step over (mm)	Stand-off distance (mm)	Nozzle length (mm)	Nozzle orifice diameter (mm)	Nozzle exit diameter (mm)	Fixture for thermal control
Tensile Sample	N ₂	400	1.38	8	2	1.2	12	120	2	6.3	Insulated
Compressive Sample	N ₂	400	1.38	8	10	1.2	12	120	2	6.3	Water-cooled

used for the experiments. The thermal energy of the system was increased by decreasing the nozzle speed and the substrate was placed on an insulated fixture to achieve tensile residual stress in the substrate surface at the interface. In contrast, the nozzle speed was increased to obtain compressive residual stress and the Mg alloy substrate was placed on a water-cooled setup during coating (Fig. 2a) [29]. Finally, the coated samples were polished and successively ground with a series of 600, 800, 1000, and 1200 US grit SiC grinding papers to achieve a uniform coating thickness of 140 μm with a minimum surface roughness of 2.1 ± 0.15 μm (refer Fig. 2b).

2.4. Quantifying residual stresses in tensile and compressive samples

A Sint Technology hole drilling machine (Restan MTS-3000) was used to measure the residual stress. In this machine, the strain relaxation through the depth of the samples was recorded during material removal at a high speed of 400,000 rpm using a carbide cone drill bit, which did not induce residual stress in the sample. Conventional Fras-2 three-element strain gauge rosettes (Hoskin Scientific Limited) were mounted on the cleaned surface to measure the strain during the hole drilling process. The measurements were conducted to a depth of 1.8 mm in 66 successive increments with a 3-s delay between the drilling steps for

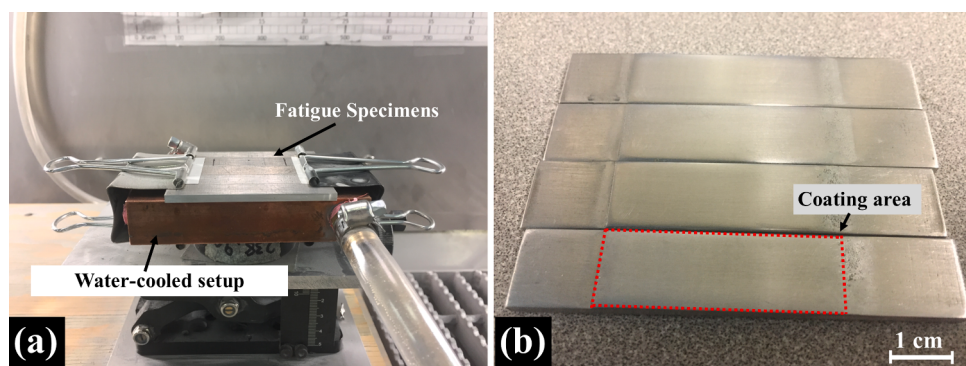


Fig. 2. a) AZ31B-H24 Mg samples placed on a water-cooled setup during cold spray. b) Coated samples for fatigue testing.

cooling and updating the strain gauges outputs. Finally, the residual stress of the coated samples was calculated using the ASTM E837-13 following the non-uniform methods [36]. For calculating the residual stress of two parts, namely coating and substrate with different materials, the material properties (Young's modulus, yield strength, and Poisson's ratio) of the coating and substrate were separately considered with respect to the exact value of the coating depth.

2.5. Fatigue tests

The three-point bending fatigue test was conducted to evaluate the surface treatment of the coated samples and compare the fatigue behavior and life of samples fabricated using different coating conditions. The maximum stress was observed at the surface during these tests. Therefore, crack initiation at or within the proximity of surface with the sub-millimeter coating was expected. An Instron 8872 servo-hydraulic axial test machine equipped with a three-point bend test fixture was used to conduct the fatigue test. The load capacity of the machine was ± 25 KN. The tests were conducted at ambient temperature (23°C). The supporting span of the samples for the three-point bend test was determined with respect to the thickness of the sample in accordance with the recommendations of the ASTM D5947 test method. The bending tests were conducted with an R-ratio of 0.1. A frequency of 1 Hz was selected for the low cycle fatigue tests, whereas a frequency of 2 Hz was selected for high cycle fatigue tests. The three-point bend tests were performed on the three types of samples at the same load levels. The three types of samples were, stress-relieved Mg samples without coating (baseline), coated tensile samples, and coated compressive samples. The experiments were performed until failure of the samples was observed, and the life of the samples was reported as the number of cycles required for rupture. The maximum applied load was adjusted at each load level to maintain the desired load level of the coated and uncoated stress-relieved samples in the same range. It should be noted that AZ31B Mg sample experiences a sharp transition from finite life to infinite ($>10^7$ cycles) life [37–40]. Therefore, load levels lower than that of the load at the transition region does not cause failure. These observations for the uncoated stress relieved samples were used to select the load levels to ensure that the samples failed during the fatigue tests at the areas of interest, i.e., coating and coating/substrate. A small load was applied to at the beginning of the tests to ensure effective contact between the sample and fixture. Fig. 3a shows the three-point bend fixture, and Fig. 3b and c depict the position of samples during the tests.

2.6. Material characterization

A scanning electron microscope (SEM) TESCAN VEGA3 equipped with an e-Flash Bruker Energy-Dispersive X-ray Spectroscopy (EDS) was used to analyze the fracture surface and observe the polished cross-

section of the coated samples. The EDS map of the fracture surfaces was used to determine the locations of the coating and substrate boundary, and cracks.

Transmission electron microscopy (TEM, JEOL-2010F) was used to investigate the interface of the coated samples (between the coating and substrate). The TEM sample was prepared using a focused ion beam (FIB, Zeiss NVision40), which was combined with a Schottky field emission 200-keV SEM.

Computerized micro-scale tomography (CT) scans were made using a ZEISS Xradia 520 Versa 3D X-ray microscope (ZEISS, Oberkochen, Germany) with a voxel size of $3.5\text{ }\mu\text{m}$ to study crack locations prior to sample failure. A representative volume element with dimensions of $1.8 \times 1.3 \times 3.26\text{ mm}$ was specified for the scanning to identify defects in the coated samples.

Digital image correlation (DIC, Correlated Solution co.) was used to capture crack initiation positions and monitor their propagation in the coated samples during fatigue testing.

The crack propagation in the fractured samples was investigated by cutting the samples perpendicular to the fracture surface to observe the cross-section. Subsequently, the cross-section was mechanically ground using a SiC sandpaper (1200 US grade) and polished using a $0.05\text{-}\mu\text{m}$ SiC suspension. The samples were etched with Keller's reagent (ES Laboratory, LLC) for 20 s to reveal the microstructural grains and boundaries of the AA7075 coating.

3. Results and discussion

3.1. Residual stress measurements

Controlling the thermal history during the coating process provided various conditions for desirable residual stress distributions in the coating and substrate [23,29]. Two types of coating procedures were performed for eight AZ31B Mg substrates with a thickness of 3.16 mm based on the design of the experiment discussed in section 2.2. Four samples with low thermal energy input (tensile samples) and four samples with high thermal energy input (compressive samples) were used. Considering the coating parameters and process discussed in section 2.3, two different coating thicknesses (approximately 350 and 200 μm for tensile and compressive samples, respectively) were fabricated. Subsequently, the samples were polished to obtain a thickness of 180 μm . Fig. 4 depicts the measured average residual stress profiles of the two types of samples. In the case of compressive samples, significant compressive residual stress was induced on the coating and substrate sides of the interface. A smooth transition to tensile residual stress at a distance from the interface was observed. Conversely, in the case of tensile samples, the transition from compressive residual stresses to tensile stress occurred in the coating area close to the interface. Hence, tensile residual stresses were induced in the substrate. Moreover, lower

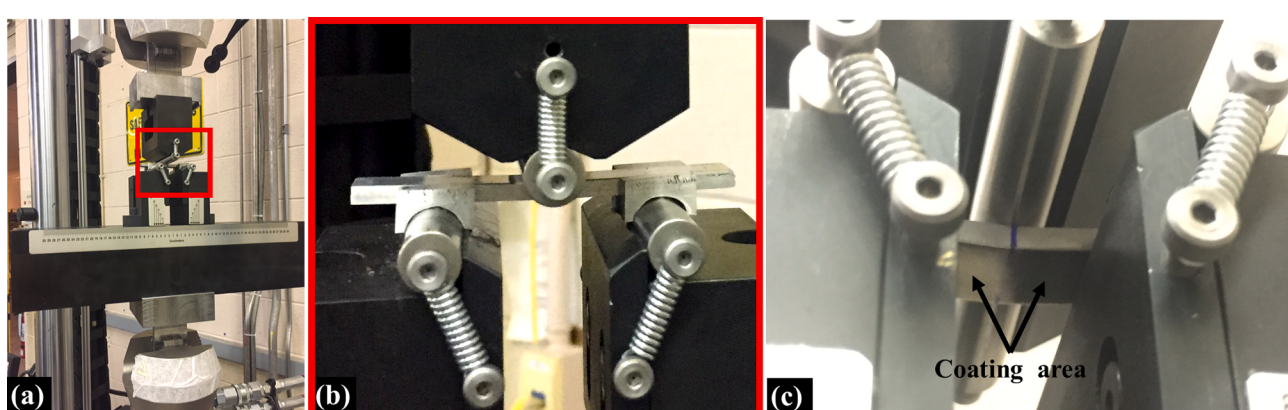


Fig. 3. a) Three-point bend test setup. b) Closeup details of sample. c) Loading and coated face.

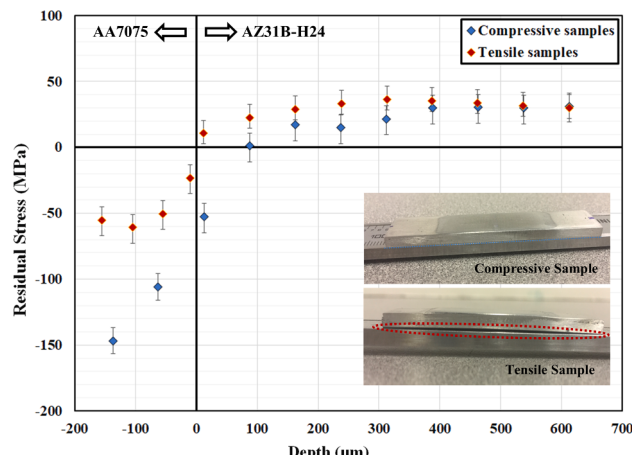


Fig. 4. Residual stress distribution in tensile and compressive samples.

compressive residual stresses were induced in the coating of the tensile samples compared with that of the compressive samples. A maximum compressive residual stress of -60 MPa was recorded at approximately $100\text{ }\mu\text{m}$ below the coating surface of the tensile samples, whereas the maximum compressive residual stress in the compressive sample was -147 MPa and at the coating surface. A tensile residual stress of 11 MPa was measured at the interface of the tensile samples on the Mg side, while the residual stress for compressive samples at the same location decreased to -53 MPa. The lower coating temperature and higher heat transfer due to the water-cooled setup led to substantial compressive residual stress owing to the cold spray peening effect, which reduced the detrimental effect of Mg/Al thermal mismatch on residual stress in the compressive samples [29]. The higher thermal expansion coefficient of the Mg substrate ($26 \times 10^{-6}/^\circ\text{C}$) compared with that of the Al coating ($23.2 \times 10^{-6}/^\circ\text{C}$) resulted in the development of higher thermal tensile stress in the coating due to the lower substrate temperature than that of the coating during the process [21–22]. Hence, the higher coating temperature facilitated bonding in the tensile samples compared with that of the compressive samples, as observed from the curvatures of tensile and compressive samples after the coating process (Fig. 4, inset images).

3.2. Fatigue of coated samples

The three-point fatigue bending tests were performed on the coated samples, both tensile and compressive, and on the stress-relieved AZ31B-H24 (baseline) samples without coating. The tests were performed in load control mode by selecting three maximum load levels of 465 , 575 , and 810 N to achieve three load amplitude levels to obtain fatigue lives in the range of 10^3 – 10^5 for the baseline sample. A minimum of three replicates were tested at each load level for the samples. Loads lower than 465 N did not cause failure of the three types of samples. Conversely, loads greater than 810 N considerably reduced the life of the samples (lower than 1000 cycles). These same load amplitudes were used in fatigue tests of tensile and compressive samples. However, these load amplitudes resulted in different stress amplitudes in tensile and compressive samples compared with that of the baseline samples due to the composite nature of coated samples.

The elastic flexure formula for composite beams was employed to calculate the stress amplitudes during the fatigue testing of the coated samples [41]. The thickness of the sample was increased only by 4.5% after depositing a $140\text{-}\mu\text{m}$ AA7075 layer on the substrate. However, the effect of the thin layer was significant in terms of changes in stress and fatigue strength owing to the different material properties of the deposited layer. The substrate and coated part exhibited different stress distributions. The transformed section method was used to obtain an

equivalent cross-section for the coated samples based on the ratio of the substrate to coating elastic modulus, which was subsequently used for stress calculations. The actual maximum stress amplitude of the coated samples was calculated using this method.

Fig. 5 depicts the load-life and stress-life (S-N) results obtained after performing fatigue tests. The data presented in Fig. 5a shows that the fatigue life of the tensile samples was less than that of the stress-relieved samples under the load amplitude of 210 N, whereas the compressive samples exhibited significant improvement in the fatigue life at the same load level. More precisely, at the load amplitude of 210 N, the average fatigue life of the uncoated samples was $38,830$ cycles. Whereas the average fatigue life of the tensile samples was $16,590$ cycles, which demonstrated a 57% reduction in their life. In contrast, the compressive samples with an average life of $89,240$ demonstrated an improvement of 130% . Different trends were observed at a higher load amplitude level of 365 N. The fatigue life of the tensile and compressive samples tested at this load amplitude was reduced by 78 and 47% compared with that of the uncoated samples, respectively (Fig. 5a). The load amplitude was sufficient to induce a displacement of 1.2 mm during the first cycle of testing (Fig. 6). It can be observed from Fig. 5a that the fatigue life of coated samples in the low cycle regime was decreased regardless of the residual stress in the samples. Similar observations have been reported in the literature [42], wherein it was reported that the cold spray coating could improve the fatigue strength by delaying the crack initiation at a low level of stress, but less or negligible improvement was observed at low lives. However, a realistic comparison was performed when the load-life raw data was transferred to stress-life for the uncoated and coated samples. Fig. 5b depicts the stress-life results. It can be observed that the coated samples exhibited higher stress when the material change was considered during the stress calculation. Fig. 5b shows that the fatigue life of the tensile samples was close to that of the fatigue life of stress-relieved AZ31B at a maximum stress of approximately 377 MPa. However, the life of the compressive samples at the same stress level was increased from approximately 4000 cycles to $18,000$ cycles, which demonstrated an improvement in their life by a factor of 4.5 .

Table 3 lists the stress induced due to loading on the surface of the coating and interface of the tensile and compressive samples at a maximum stress of 290 MPa. In addition, Table 3 presents the measured residual stress on the surface and at the interface of the tensile and compressive samples along with the net stress at each location. The calculated maximum applied stress on the surface of the tensile and compressive samples were 300 and 306 MPa, which were 16 and 18% greater than that of the AZ31B samples, respectively. However, considering the residual stress in the samples, the resultant stress reduced to 245 and 159 MPa for tensile and compressive samples, respectively. Hence, the maximum stress at the surface of the compressive sample at the beginning of the fatigue tests was 38.6% less than that of the AZ31B sample under the same load amplitude. Therefore, the compressive samples were expected to have a higher fatigue life due to the higher fatigue strength of the AA7075. Additionally, these samples exhibited lower stresses compared with that of the uncoated AZ31B samples.

The deformation of the samples during the fatigue test was studied to investigate the failure of the tensile and compressive samples. Fig. 7 shows the maximum and minimum displacement of a tensile and a compressive sample versus the normalized number of cycles extracted from the data recorded during the three-point bending test. The number of cycles was normalized to compare the displacement obtained from the two types of coated samples with different fatigue lives using the following equation:

$$\text{Normalized life} = \frac{\text{cycle number}}{\text{Cycle number at failure}} \times 100.$$

Different trends were observed for the maximum and minimum displacements of the tensile and compressive samples at the same load amplitude of 210 N (refer Fig. 7). The displacement curves of the tensile

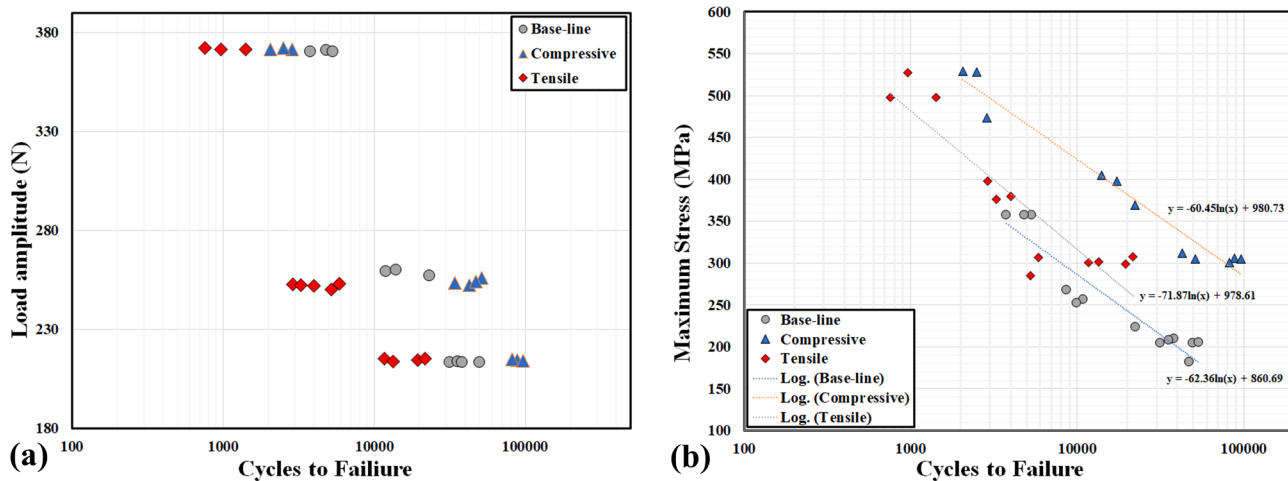


Fig. 5. a) Fatigue test results for uncoated, tensile, and compressive samples. b) Fatigue test results for uncoated, tensile, and compressive samples calculated by considering the coated samples as composite beams.

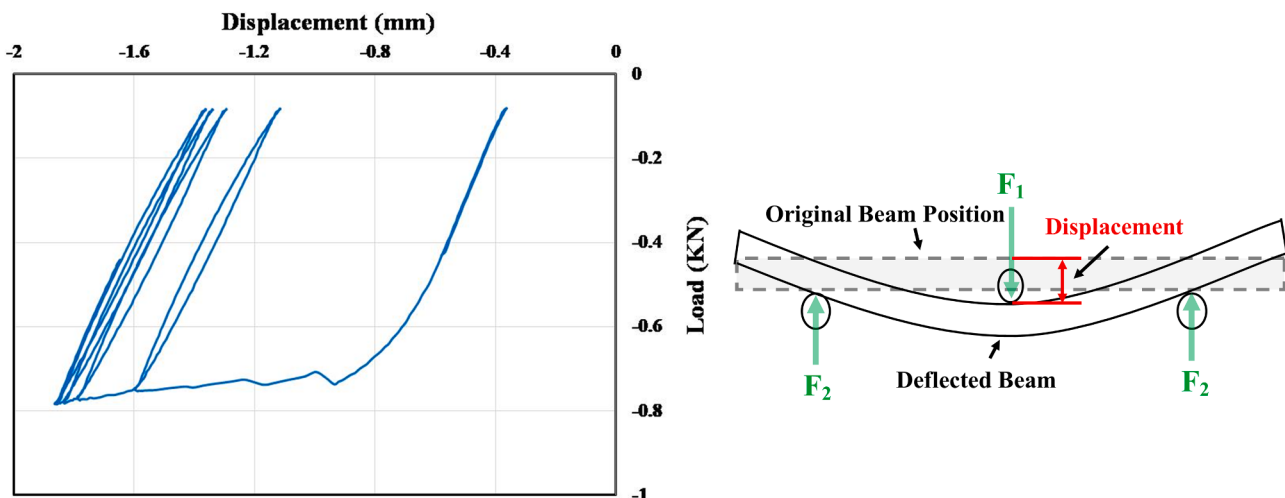


Fig. 6. Applied load versus beam maximum deflection for the first five cycles of a tensile sample.

Table 3

Typical stress condition at the surface and interface of coated and uncoated samples, and their corresponding cracking mechanism as observed at a maximum stress of 290 MPa.

Material	Tensile Samples			Compressive Samples			AZ31B Samples (baseline)
	Interface	Surface	Interface	Surface	Surface	Surface	
	AA7075	AZ31B	AA7075	AA7075	AZ31B	AA7075	
Applied max stress (MPa)	271	198	300	278	201	306	259
Residual stress (MPa)	-23	11	-55	-80	-53	-147	0
Combined stress (MPa)	248	209	245	198	148	159	259
Number of cycles to failure	12,910			72,365			9866
Crack initiation site	Interface			Surface			Surface

sample increased when it reached 90% of its life (point A). The fatigue cracks cannot be observed by the DIC camera in this situation, which was used for monitoring the crack on the coating surface of the tensile sample. However, the response of the sample according to the applied load was changed. Therefore, the change in the tensile sample displacement and its gradual increase at point A (shown in Fig. 7) might exhibit cracking of the sample at the coating and substrate interface. In contrast, the compressive sample did not exhibit this relatively long-term degradation for 90% of life to final failure. However, it failed fast at the end of the experiment, as shown in Fig. 7 (point B). Fatigue

cracks appeared immediately on the coating surface of the compressive samples when the displacement response to the loading of the compressive samples changed and were detected by the DIC. Fig. 8a shows an example of the fatigue cracks at the coating surface of compressive samples when the displacement response of the sample started to change. Therefore, it was observed that the fatigue failure mechanisms of the tensile and compressive samples were different.

The tests were immediately stopped after the displacement curves exhibited deviation from their steady-state at Points A and B (Fig. 7) to investigate fatigue crack initiation in the coated samples. Fig. 8b depicts

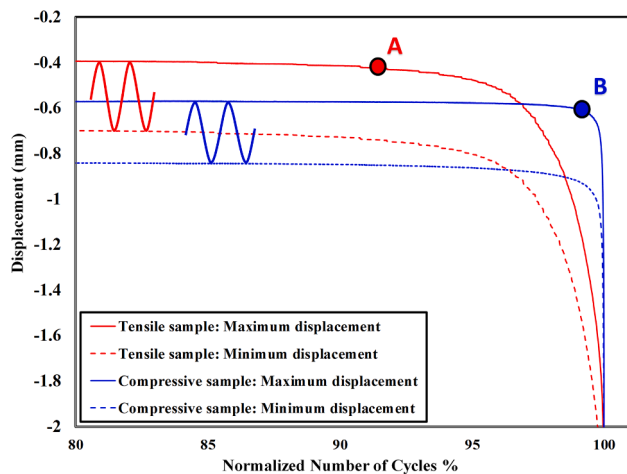


Fig. 7. Maximum and minimum deflection of coated samples during the three-point bend tests versus the normalized life at a load level of 210 N.

the fatigue crack on the coating surface of the compressive sample before the failure occurred at point B. The samples were cut perpendicular to the crack propagation direction and polished to observe the cracking process. Fig. 8c shows the cross-section of the coated sample,

which represents the fatigue crack that developed in the coating, crossed the interface, and propagated into the substrate.

In contrast, surface cracks were not detected by the DIC when the fatigue test of the tensile sample was stopped at approximately 90% of its expected fatigue life (point A in Fig. 7). A micro-CT scanning was performed to investigate the possibility of crack initiation inside the sample before cutting to examine the presence of a sub-surface crack in the sample. The CT scan image of the sample exhibited cracks and/or potential delamination at the interface of the coating and substrate (Fig. 9a). subsequently, the sample was sectioned from the mid-span and polished for SEM observation to confirm the presence of a crack at the interface. Fig. 9b shows the presence of fatigue cracks in the AA7075 close to the interface. The presence of trapped particles detected near the interface of tensile samples might be a cause of crack initiation/delamination in this area. The undeformed particles (trapped particles) had a lower particle velocity compared with that of the critical velocity of particles during the coating deposition due to their particle size. Therefore, the kinetic energy of the particles was inadequate to cause deformation.

The fractured surfaces of the tensile and compressive coated samples were studied after fatigue failure. Fig. 10a and c depict different fracture surfaces for the tensile and compressive samples, respectively. The fracture surface of the tensile sample demonstrated that cracks in the sample were developed with an angle with respect to the fracture surface (Fig. 10a). Fig. 11a shows the high-resolution image of such a crack

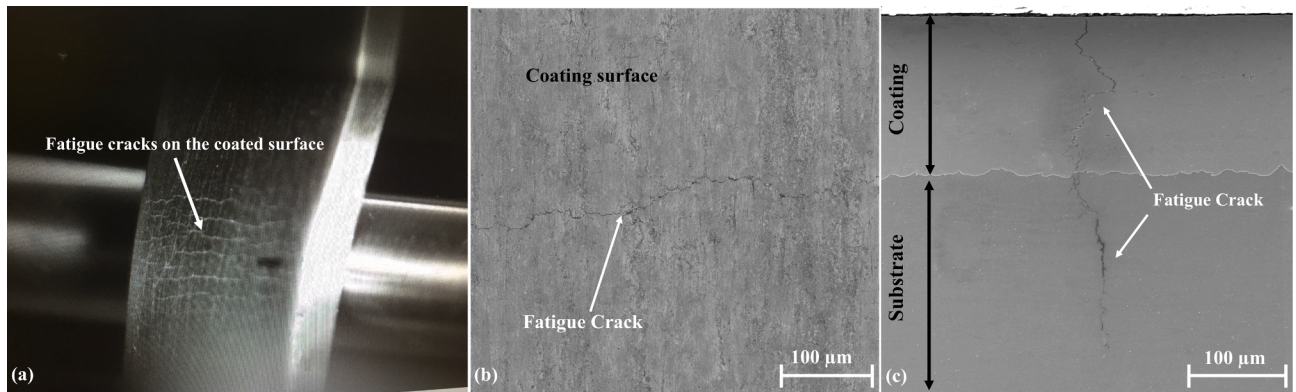


Fig. 8. a) Fatigue cracks initiated at the coating surface of the compressive sample when the displacement of the sample significantly increased (before final failure at point B in Fig. 7). b) Magnified image of the fatigue crack observed at the top surface of the compressive sample. c) Fatigue crack in the cross-section of the same compressive sample exhibiting the advancement of crack into the substrate from the coating.

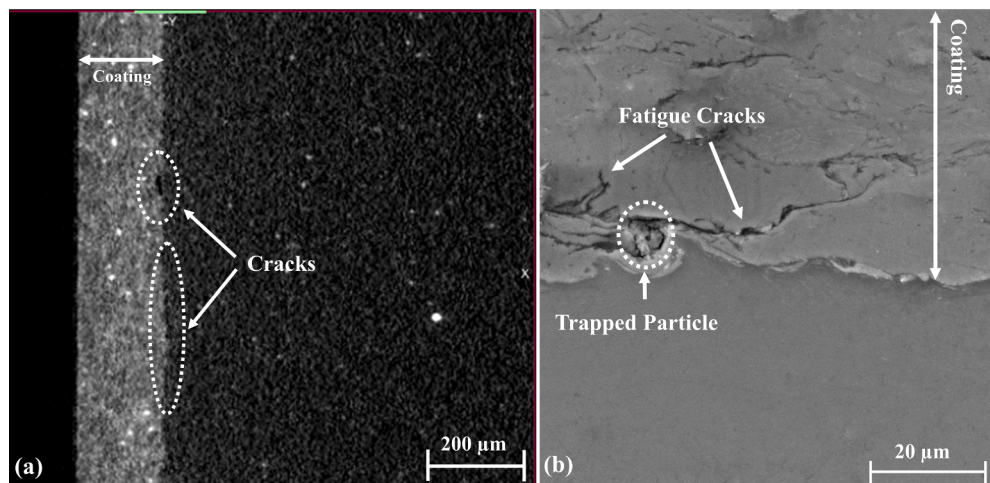


Fig. 9. a) CT scan image of the cross-section of the tensile sample after 90% of its fatigue life. Two separate cracks initiating at the interface were observed. b) Crack initiation at the interface in the cross-section of the tensile sample at point A (Fig. 7), which exhibits crack initiation from a trapped particle at the interface.

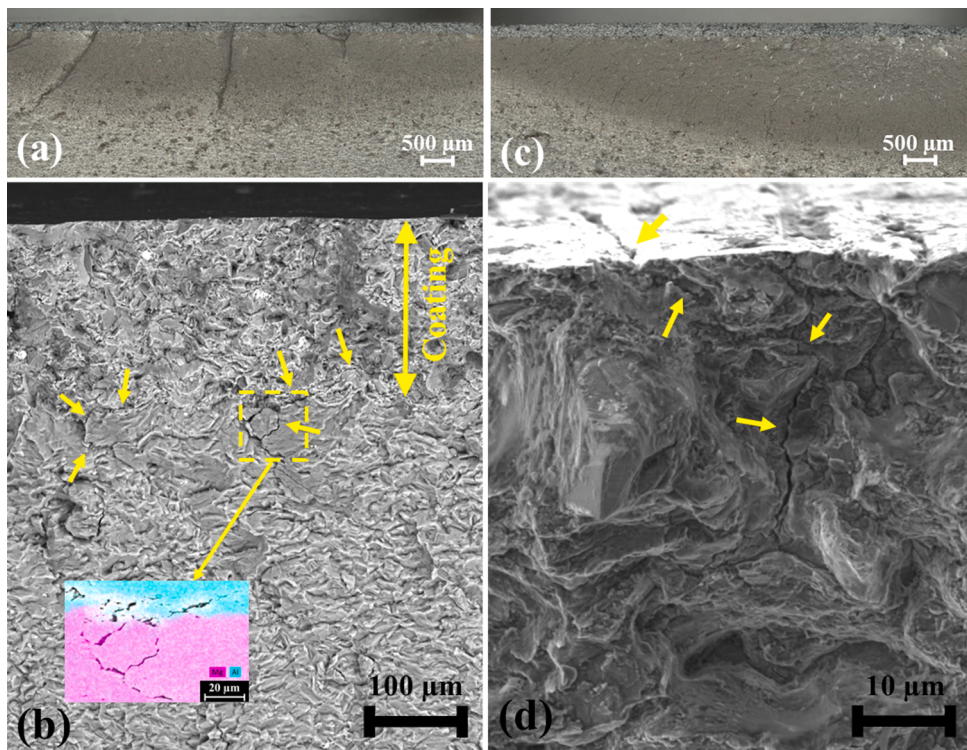


Fig. 10. a) Fracture surface of the tensile sample showing multiple crack paths. b) Crack propagation in the tensile sample. The inset is EDX analysis confirms that the crack was located at the interface of Al and Mg. c) Fracture surface of the compressive sample. d) Cracks at the surface of the compressive sample.

on the surface. These images depicted that the crack initiated close to the interface, propagated at an angle to the fracture surface, and left marks

on the surface. Fig. 10b depicts crack propagation in the AA7075 close to the interface and propagation to the Mg substrate. The cracks were marked with arrows in the image. In addition, the EDX elemental map of the marked area was added to the image as an inset, which verified the propagation of the crack from the interface to the substrate and coating of the tensile sample. In contrast, the fractography of the compressive sample (Fig. 10c) revealed a typical fatigue fracture surface. Fig. 10d shows the cracks at the surface of the compressive sample that propagated in the coating (arrows point the position of the cracks) and continued to the interface and substrate (Fig. 11b).

Further examination of the fractured samples was performed to investigate the crack propagation mechanism within the coatings. The fractured samples were cut perpendicular to the fracture surface to enable observation of failure within the coatings. Fig. 12 shows such a surface in the tensile and compressive samples, wherein fatigue cracks propagated in the AA7075 coating. Fig. 12a, c, and e revealed that the cracks propagated through the splats (intra-splats) in the tensile samples. Whereas the fatigue cracks propagated through the splat boundaries (inter-splats) in the compressive samples, (Fig. 12b, d and f). The reason for these two different crack propagation mechanisms is described as follows. The fatigue cracks initiated from the surface of the compressive samples and gradually propagated into the coating. Therefore, the inter-splat crack propagation mechanism was probable due to the lower strength of the splat boundaries than that of the strength of the grains. Conversely, the fatigue crack initiation in the tensile samples occurred at the interface and subsequently propagated to the substrate and coating. Considering the lower fatigue strength of the substrate compared with that of the AA7075 coating, fatigue cracks are expected to propagate initially into the substrate. Hence, the failure in the coating might have occurred at the last stage of the fatigue failure (tearing off), wherein the stress at the crack tips was sufficient to allow propagation to the splats and through the grain boundaries.

The results of crack initiation during the fatigue test using different techniques, such as DIC (visual in-situ inspection during the fatigue test), optical microscopy, CT scanning, and SEM microscopy, confirmed

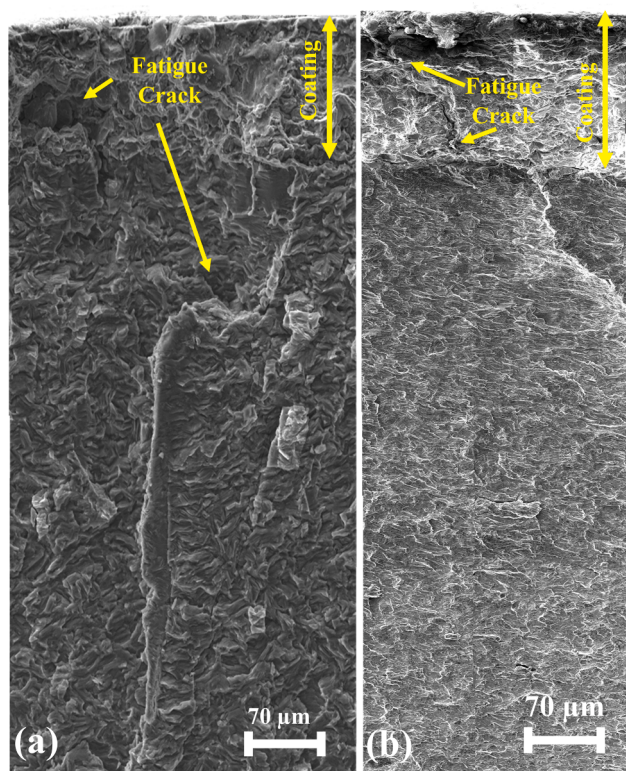


Fig. 11. Fatigue crack initiation and propagation through the AZ31B substrate of a) the tensile sample exhibiting multiple cracks, b) the compressive sample exhibiting surface crack propagation path.

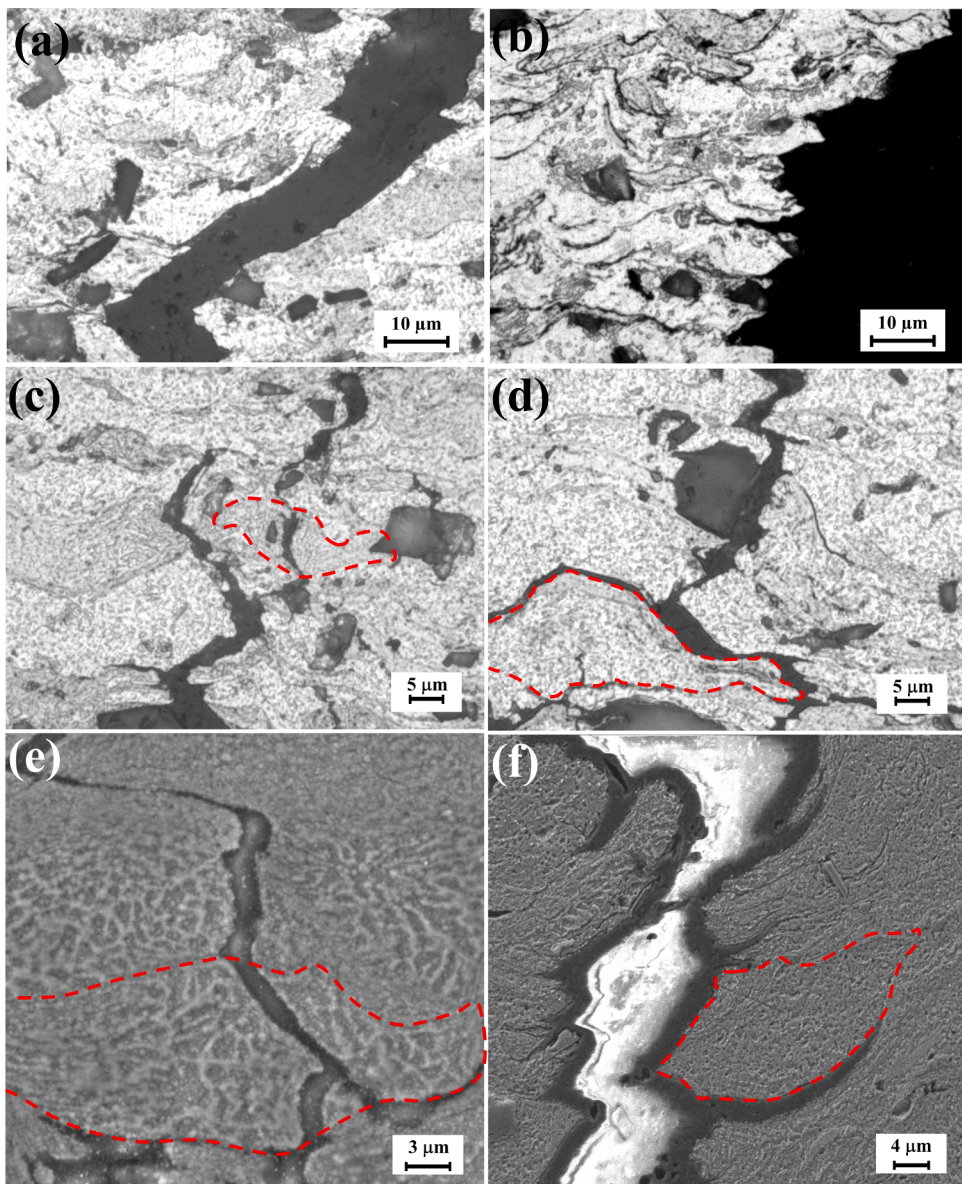


Fig. 12. Crack propagation in the AA7075 coating for: a, c, e) the tensile sample, which exhibits intra-splat (transgranular) crack propagation mechanism in the coating; b, d, f) the compressive sample, which exhibits inter-splat crack propagation mechanism.

that the mechanisms of fatigue crack initiation for the tensile and compressive samples were different. There are multiple reasons that might have caused the difference in the fatigue crack initiation mechanisms.

Depositing a thin layer of material with an elastic modulus higher than that of the substrate, AA7075 on AZ31B in this case, changed the uniform stress distribution in the cross-section of the composite beam under bending. The stress calculations provided in Table 3 suggest that the coating decreased the initial applied stress on the substrate at the interface compared with that of the uncoated samples. However, a higher stress was applied on the coating at the interface and on the coating surface. This stress distribution interfered with the applied residual stress induced in the samples during coating. In the case of the compressive sample, the induced residual stress at the interface decreased the total stress at the interface region, which consequently decreased the probability of crack initiation or propagation at the interface. Conversely, in the case of tensile samples, the applied stress on the coating side of the interface was expected to be significantly higher than that of the compressive sample. For example, in the case reported in

Table 3 for the tensile sample, the applied stress on the coating side of the interface was significantly close to the applied stress at the surface of this sample. This increased the probability of crack initiation at the interface compared with that of the top surface of the coating, wherein the maximum stress was expected.

On the other hand, the microstructural characteristics of tensile and compressive samples supported a higher tendency of crack initiation at the interface for the tensile sample compared with that of the compressive samples. Fig. 13a and b depict a nano-size interlayer formed at the interface of Mg and AA7075 with a columnar grain morphology during cold spray coating. A similar nano-sized interlayer has been reported by Wang et al. [43], and Shaha and Jahed [44,45] for Mg coated with Al. This area consisted of a mixture of Al and Mg formed by Al diffusing into the Mg substrate. The size of this area was approximately four times larger in the tensile sample compared with that of the compressive sample. Defects, such as voids generated due to the mismatch of thermal expansion (because of the carrier gas temperature) of Al and Mg, and the higher rate of diffusivity of Al compared with that of Mg, have been reported [44]. It can be traced at the grain boundaries

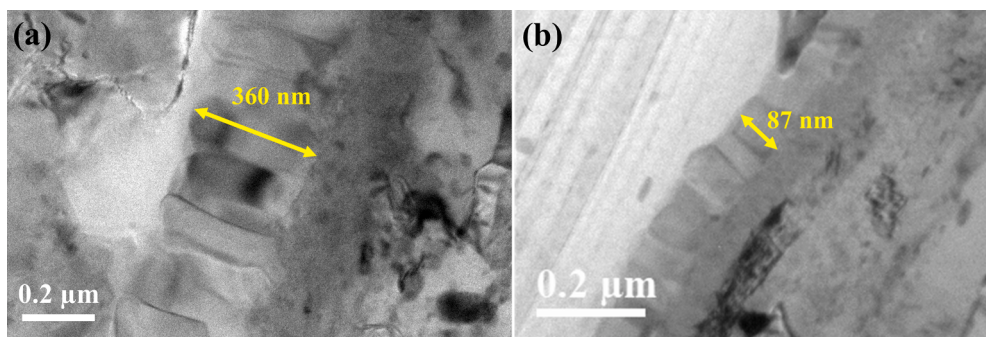


Fig. 13. TEM image of the nano-size interlayer at the interface between Mg and AA7075 in cold spray coating with a columnar grain morphology. a) Tensile sample exhibiting a significantly larger interlayer of 360 nm. b) Compressive sample exhibiting a smaller interlayer of 87 nm. The TEM samples are prepared immediately after the coating and before loading.

of the columnar grains in the nano-size interlayer shown in Fig. 13. The volume fraction of these defects at the interface was larger in the tensile samples, which can lead to a higher tendency of crack initiation through coalescence of voids. Moreover, Marzbanrad et al. [29] reported that the local microstructure of Mg substrate adjacent to this interlayer area exhibited significantly coarser grains in the tensile sample compared with that of the compressive samples (the average size of grains in the compressive sample in this area was five times larger than that in the tensile sample). This can lead to premature crack initiation at the interface in the tensile sample under the same stress conditions.

Therefore, considering the stress levels and the microstructural features, crack initiation and propagation in the tensile sample occurred at the interface and the cracks propagated to the Mg substrate before extending to the coatings. Conversely, the crack initiation had a significantly higher probability at the coating surface, and it propagated toward the interface in the compressive samples. This result was verified using DIC in-situ crack monitoring, CT scan of the tensile sample before failure, and fracture surface analysis.

4. Conclusion

AZ31B Mg sheets coated with AA7075 were fabricated using two different cold spray coating conditions to induce tensile and compressive residual stresses in the substrate near the interface. The fatigue performance of the samples was assessed using three-point bending fatigue tests. The conclusions of this study are as follows.

- (1) The average fatigue life of the compressive samples at a stress of 377 MPa was greater by a factor of 4.5 compared with that of the uncoated AZ31B samples at the same stress. However, the average fatigue life of the tensile sample did not exhibit a significant change compared with that of the stress-relieved AZ31B samples at the same stress.
- (2) In the case of compressive samples, the fatigue crack initiation occurred at the coating surface of the sample and the cracks propagated through the coating into the substrate, which resulted in the failure of the sample.
- (3) The fatigue crack in the tensile sample was initiated from the coating-substrate interface and propagated along the interface, toward the substrate and coating.
- (4) The fatigue cracks were propagated through the splat boundaries of the cold spray coated AA7075 compressive samples, which demonstrated an inter-splat propagation mechanism, whereas an intra-splat (transgranular) crack propagation was observed in the coating of the tensile samples.
- (5) The stress analysis using the composite beam theory confirmed that the initial stress state in the tensile and compressive samples were significantly different. The stress level at the coating surface and interface of the tensile sample was comparable. However,

this was not the case in the compressive sample. The stress at the interface was significantly lower than that on the coating surface due to the presence of compressive residual stress at the interface.

- (6) This research demonstrated that by selection of proper cold spray coating parameters compressive residual stress can be induced at interface. The residual stress distribution can be adjusted along with the microstructural refinement at the interface to enhance the fatigue performance of the coated sample. However, improper selection of cold spray parameters might lead to the formation of tensile residual stress at the interface, which might result in cracking and delamination of the coating at the interface. This is undesirable and might result in negligible improvement in the fatigue life.

Declaration of Competing Interest

The authors declare that they have no known competing financial interests or personal relationships that could have appeared to influence the work reported in this paper.

Acknowledgments

The financial support of the Natural Sciences and Engineering Research Council of Canada (NSERC) through the Automotive Partnership Canada (APC) under APCPJ 459269-13 grant with contributions from Multimatic Technical Centre, Ford Motor Company, and Centerline Windsor are acknowledged. Funds from NSERC-RTI program under EQPEQ458441-2014 grant also supported this research.

References

- [1] Kainer KU. Magnesium Alloys and Technologies. Wiley-VCH; 2003.
- [2] Brady MP, Joost WJ, Warren CD. Insights from a recent meeting: Current status and future directions in magnesium corrosion research. Corrosion 2017;73(5):452–62.
- [3] Kuffova M. “Fatigue Endurance of Magnesium Alloys”, in *Magnesium Alloys - Design, InTech: Processing and Properties*; 2011.
- [4] Stoud MR, Ricker RE, Cammarata RC. The influence of a multilayered metallic coating on fatigue crack nucleation. Int J Fatigue 2001;23(SUPPL. 1):215–23.
- [5] yun Bai Y, Gao J, Guo T, wei Gao K, Volinsky AA, lu Pang X. Review of the fatigue behavior of hard coating-ductile substrate systems. Int J Miner Metall Mater 202; 28(1):46–55.
- [6] Sample CM, Champagne VK, Nardi AT, Lados DA. Factors governing static properties and fatigue, fatigue crack growth, and fracture mechanisms in cold spray alloys and coatings/repairs: A review. Addit Manuf 2020;36:101371.
- [7] Ma A, et al. The fretting fatigue performance of Ti-6Al-4V alloy influenced by microstructure of CuNiIn coating prepared via thermal spraying. Tribol Int 2019; 145(December):106156.
- [8] Fajdiga G, Sraml M. Fatigue crack initiation and propagation under cyclic contact loading. Eng Fract Mech 2009;76(9):1320–35.
- [9] Moridi A, Hassani-Gangaraj SM, Vezzù S, Trško L, Guagliano M. Fatigue behavior of cold spray coatings: The effect of conventional and severe shot peening as pre-/post-treatment. Surf Coatings Technol 2015;283:247–54.
- [10] Dayani SB, Shaha SK, Ghelichi R, Wang JF, Jaled H. The impact of AA7075 cold spray coating on the fatigue life of AZ31B cast alloy. Surf Coatings Technol 2018; 337(January):150–8.

- [11] Zieman CW, Sharma MM, Bouffard BD, Nissley T, Eden TJ. Effect of substrate surface roughening and cold spray coating on the fatigue life of AA2024 specimens. *Mater Des* 2014;54:212–21.
- [12] Ghelichi R, MacDonald D, Bagherifard S, Jahed H, Guagliano M, Jodoin B. Microstructure and fatigue behavior of cold spray coated Al5052. *Acta Mater* 2012; 60(19):6555–61.
- [13] Bai Y, Guo T, Wang J, Gao J, Gao K, Pang X. Stress-sensitive fatigue crack initiation mechanisms of coated titanium alloy. *Acta Mater* 2021;217:117179.
- [14] Qian Z, Huang H. Monitoring of Crack Initiation at Coating/Substrate Interface by Residual Magnetic Field Measurement. *J Nondestruct Eval* 2021;40(2):1–11.
- [15] Sivagnanam Chandra NGP, Otsuka Y, Mutoh Y, Yamamoto K. Effect of coating thickness on fatigue behavior of TiAlN coated Ti-alloys. *Int J Fatigue* 2020;140, no. April:105767.
- [16] Bagherifard S, Guagliano M. Fatigue performance of cold spray deposits: Coating, repair and additive manufacturing cases. *Int J Fatigue* 2020;139, no. April:105744.
- [17] Tabatabaeian A, Ghasemi AR, Shokrieh MM, Marzbanrad B, Baraheni M, Fotouhi M. Residual Stress in Engineering Materials: A Review. *Adv Eng Mater* 2021;2100786:1–28.
- [18] Villafuerte J. Modern Cold Spray; Materials, Process, and Applications. Springer International Publishing; 2015.
- [19] Papyrin A, Kosarev V, Klinkov S, Alkhimov A, Fomin V. Cold Spray Technology. 1st ed. Amsterdam: Elsivier; 2006.
- [20] Assadi H, Kreye H, Gärtner F, Klassen T. Cold spraying – A materials perspective. *Acta Mater* 2016;116:382–407.
- [21] Marzbanrad B, Toyserkani E, Jahed H. Multi-Layer Cold Spray Coating: Strain Distribution. *Key Eng Mater* Jul. 2019;813:411–6.
- [22] Marzbanrad B, Toyserkani E, Jahed H. Characterization of Single- and Multilayer Cold-Spray Coating of Zn on AZ31B. *Submitt to Surf Coat Technol* 2020.
- [23] Marzbanrad B, Toyserkani E, Jahed H. Customization of residual stress induced in cold spray printing. *J Mater Process Technol* 2021;289:116928.
- [24] Diab M, Pang X, Jahed H. The effect of pure aluminum cold spray coating on corrosion and corrosion fatigue of magnesium (3% Al-1% Zn) extrusion. *Surf Coatings Technol* 2017;309:423–35.
- [25] Cavaliere P, Silvello A. Processing conditions affecting residual stresses and fatigue properties of cold spray deposits. *Int J Adv Manuf Technol* 2015;81(9–12): 1857–62.
- [26] Yuming X, Ming-Xing Z. The effect of cold sprayed coatings on the mechanical properties of AZ91D magnesium alloys. *Surf Coatings Technol* 2014;253:89–95.
- [27] Dayani SB, Shaha SK, Ghelichi R, Wang JF, Jahed H. The impact of AA7075 cold spray coating on the fatigue life of AZ31B cast alloy. *Surf Coatings Technol* 2018; 337(June 2017):150–158.
- [28] Vargas-Uscategui A, King PC, Styles MJ, Saleh M, Luzin V, Thorogood K. Residual Stresses in Cold Spray Additively Manufactured Hollow Titanium Cylinders. *J Therm Spray Technol* 2020.
- [29] Marzbanrad B, Razmipoosh M, Toyserkani E, Jahed H. Role of Heat Balance on the Microstructure Evolution of Cold Spray Coated AZ31B with AA7075. *J Magnes Alloy* 2021;9:1458–69.
- [30] Xiong Y, Zhang MX. The effect of cold sprayed coatings on the mechanical properties of AZ91D magnesium alloys. *Surf Coatings Technol* 2014;253:89–95.
- [31] Marzbanrad B, Jahed H, Toyserkani E. On the evolution of substrate's residual stress during cold spray process: A parametric study. *Mater Des* 2018;138:90–102.
- [32] Metal Handbook: 4E: Heat Treating of Nonferrous Alloys. ASM International, 2018.
- [33] Xue Y, Pang X, Jiang B, Jahed H. Corrosion and corrosion fatigue performances of micro-arc oxidation coating on AZ31B cast magnesium alloy. *Mater Corros* 2019; 70(2):268–80.
- [34] Shayegan G, et al. Residual stress induced by cold spray coating of magnesium AZ31B extrusion. *Mater Des* 2014;60:72–84.
- [35] Jahed H, Ghelichi R. Residual Stresses and Fatigue Life Enhancement of Cold Spray. In: Villafuerte J, editor. Modern Cold Spray: Materials, Process, and Applications. Cham: Springer International Publishing; 2015. p. 225–52.
- [36] Schajer GS. Measurement of non-uniform residual stresses using the hole drilling method - part I: Stress calculation procedure. *Am Soc Mech Eng Mater Div MD* 1988; 7(October): 85–91.
- [37] Guo S, Liu X, Zhang H, Yan Z, Zhang Z, Fang H. Thermographic study of az31b magnesium alloy under cyclic loading: Temperature evolution analysis and fatigue limit estimation. *Materials (Basel)* 2020;13(22):1–18.
- [38] Wang Y, Culbertson D, Jiang Y. An experimental study of anisotropic fatigue behavior of rolled AZ31B magnesium alloy. *Mater Des* 2020;186:108266.
- [39] Marzbanrad B. Behaviour of Magnesium Alloy Under Load-Control Cyclic Testing. Waterloo, Canada: University of Waterloo; 2015.
- [40] Yazdanmehr A. Modeling the Residual Stress Distribution and Experimental Characterization of Shot Peening on AZ31B Rolled Sheet Internal Member; 2020. p. 151.
- [41] Popov E. Engineering Mechanics of Solids. New Jersey: Prentice-Hall Inc; 1990.
- [42] Grrieron D, et al. Fracture and Fatigue, 2014;7:65–71.
- [43] Wang Q, Qiu D, Xiong Y, Birbilis N, Zhang MX. High resolution microstructure characterization of the interface between cold sprayed Al coating and Mg alloy substrate. *Appl Surf Sci* 2014;289:366–9.
- [44] Shaha SK, Jahed H. An in-situ study of the interface microstructure of solid-state additive deposition of AA7075 on AZ31B substrate. *Appl Surf Sci* 2020;508 (October 2019):144974.
- [45] Shaha SK, Jahed H. Characterization of nanolayer intermetallics formed in cold sprayed Al powder on Mg substrate. *Materials (Basel)*. 2019; 12(8).